

V.I. Perekrestov, Yu.O. Kosminska, Yu.V. Gannych, G.S. Kornushchenko

Regularities of Structure Formation and Physical Properties of Multilayered Composites Based on W, Ta, Hf, Ti, Mo, Cr, Al, and C

Sumy State University, Sumy, Ukraine, v.perekrestov@phe.sumdu.edu.ua

New fabrication technique of multilayered composite coatings on inner surface of pipes is developed which is based on ion-plasma sputtering of rod-like target composed of various metals and graphite. It is established that gradient change of elemental composition in the direction Cr→W→Mo→Ta→Hf→Ti→C→Ti/Al→C is accompanied by transition from metal mixture carbide to titanium carbide with the grain sizes of ~ 8 - 15 nm. It is found that increase in microhardness up to ~ 26 GPa is caused by additional surface heating by thermal radiation from the ion-heated rod and by elemental composition of the composite layers.

Keywords: multicomponent coatings, composites, carbon, carbide, elemental composition, phase composition.

Received 21 April 2020; Accepted 15.06.2020.

Introduction

Functional capabilities of protective coatings used under complex of unfavourable factors are determined by the related physical properties. The latter include a group of such characteristics as adhesion, microhardness, heat resistance, fracture strength, corrosion resistance, tribological durability, radiation resistance, etc. Monolayers of simple carbides and nitrides of transition metals cannot always provide the whole set of the mentioned properties. That is why there is a modern trend in development of ion-plasma technologies which is based on formation of multilayered and multicomponent coatings at the same time [1-5]. Their efficiency is explained by capability of different interlayers of a composite to support high adhesion combined with high antifriction characteristics while maintaining proper level of microhardness, strength and resistance to various external impacts of the coatings. At the same time in order to avoid cleavage and cracking of the coatings, it is necessary to secure decrease and delocalization of intrinsic mechanical stress.

To start, let us consider existing approaches to fabrication of multicomponent coatings with emphasis on magnetron sputtering. In [6-8] single-layered multicomponent (CrNbTaTiW)C coatings have been

fabricated by means of traditional magnetron sputtering of a composite target Ta/W (1:1), alloyed Ti/Cr (1:1) target and two separate Nb and C targets. At the same time structural studies of the obtained coatings reveal possibility of enhancing their functional characteristics owing to segregation and clusterization of constituent metals [6], and increase in deposition temperature to 600 °C and in concentration of Ta and W increases coating hardness to 36 GPa [7]. Also, multielement (TiZrNbHfTa)N and (TiZrNbHfTa)C coatings have been fabricated by traditional magnetron sputtering of targets composed of Ti, Zr, Nb, Hf and Ta in the gas mixture of Ar + N₂ or Ar + CH₄ [9-10]. Comparative analysis of the obtained nitrides and carbides [9-10] indicates their approximately similar microhardness (34 GPa for the nitride and 31 GPa for the carbide). However, the friction coefficient of the nitride coatings is almost six times higher than that of the carbide coatings which shows advantage of the latter.

As shown in [11], high-entropy carbide coatings with microhardness of 43 - 49 GPa can be fabricated by magnetron sputtering of multicomponent alloy TiZrHfVNbTa in Ar + C₂H₂ atmosphere even under relatively low substrate temperatures (~ 260 - 280 °C). It should be noted that the hardness of such coatings exceeds the hardness of the metal monocarbides that the

alloy is composed of, and the friction coefficient is relatively low (0.14 - 0.16) [11]. Also, such multicomponent coatings as $(\text{TiHfZrVNb})\text{N}$, $(\text{Ti,Zr})_{0.54}\text{Al}_{0.46}\text{N}$, and $(\text{TiZrHfVNbTa})\text{N}$ can be used as materials resistant to high-energy electrons and ions [12-14] that reveals their application and radiation resistant materials.

As a next step to further enhancing of functional possibilities of the coatings, their formation based on simultaneously multicomponent and multilayered composites should be mentioned. Now fabrication of such sophisticated coatings is somehow limited by absence of appropriate specialized technologies. In some cases, to obtain multilayered TiN/TiAlN , $(\text{TiZrNbHf})\text{N/MoN}$ and $(\text{TiN-Cu})/(\text{AlNbTiMoVCr})\text{N}$ nitride composites, two plasma arc sputterers of alloyed multicomponent targets are used in presence of nitrogen [2-5]. It should be noted that this technology allows producing coatings only of two types of interlayers. At the same time, it is established that functional capabilities of the composites produced under the above conditions are more advantageous than those of coatings produced on the basis of nitrides of single metals constituting the composite or on the basis of single-layer coatings composed of elements of any single interlayer of the composite [2-5].

Thus, one can state that fabrication of simultaneously multicomponent and multilayered composites as well as development of the related technology has high prospect of practical application. Enhanced functional characteristics can be reached if using such constituents as W, Hf, Ti, Ta, Mo, Cr, and carbon. Besides, to increase heat resistance, Al is desirable as an additive [15]. It should be mentioned that as for today the problem of deposition of the above coatings onto inner surface of low diameter pipes is still not solved properly. Hence, assuming all stated above, the main goal of the given work is to develop the technology of fabrication of simultaneously multicomponent and multilayered gradient coatings with gradual changing of elemental composition in the direction $\text{Cr} \rightarrow \text{W} \rightarrow \text{Mo} \rightarrow \text{Ta} \rightarrow \text{Hf} \rightarrow \text{Ti} \rightarrow \text{C} \rightarrow \text{Ti/Al} \rightarrow \text{C}$ deposited onto inner surface of low diameter pipes.

I. Experimental procedure

To fabricate the composites based on W, Ta, Hf, Ti, Mo, Cr, Al, and C, we have used a specially developed sputterer of a rod-like target placed inside a metallic pipe of 39 mm in diameter coaxially to it. The rod has been composed of discs of different metals, BT6 alloy (State Standard 19807-91), and graphite (see Fig. 1a). The sputterer operates on argon ions bombardment of the rod surface which is 115 mm in length and 11 mm in diameter. The rod is sputtered effectively because of hollow cathode effect and magnetron effect [16, 17]. As follows from pyrometric measurements, if the discharge power is ~ 380 W, then the rod is heated up to $\sim 540 - 680$ °C under ions action (Fig. 1b). Hence, low melting temperature of Al makes it impossible to use Al discs in the rod. Instead, a BT6 alloy disc has been used as a composing part of the rod since BT6 has Al in its

composition.

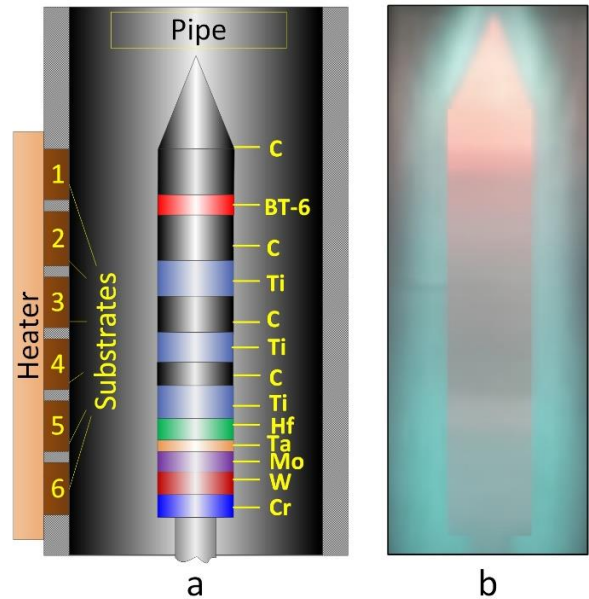


Fig. 1. Schematic representation of the sputtered rod-like target composed of different metals, BT6 alloy and graphite (a); real image of the target during sputtering (b).

All the experiments on coatings deposition onto sodium-calcium glass, fresh KCl cleaved facets and P6M5K5 steel (State Standard 19265-73 have been carried out using argon as a working gas deeply purified by the technique described in [18]. The working gas pressure has been 5 Pa, and partial pressure of all residual reactive gases has been $8 \cdot 10^{-8}$ Pa [18].

In the first series of experiments the condensates have been deposited onto KCl monocrystal cleaved facets for later transmission electron microscopy studies (TEM). In this case mutual location of the pipe with the substrates and the rod-like target corresponded to the schematic image in Fig. 1a. This location remained unchanged during deposition. Thus, the thin films possessed elemental composition that correlated with elemental distribution within the rod. Under the substrate temperature 280 - 320 °C and deposition time 80 s the thickness of the films reached $\sim 50 - 90$ nm.

In the second series of experiments the condensates have been deposited onto sodium-calcium glass substrates for later XRD studies by means of diffractometer ДРОН-4 and EDX-analysis of elemental composition with the help of scanning electron microscope Inspect S50-B (SEM). Besides, elemental composition was studied under electron energy of 10 keV. To implement this series of experiments, at first, the upper edge of the substrate #1 and the pipe was placed at the level of the lowest disc of Cr (see Fig. 1). After that the substrates were heated to ~ 320 °C, the sputterer was turned on, and the pipe together with the substrates were moving during 30 min until reaching the location shown in Fig. 1a. Then the coatings were being deposited onto the substrates during 3 h without moving the pipe relative to the rod. As in the first series of experiments, the fabricated coatings had different elemental composition but considerably higher thickness

Table 1

Elemental composition of the coatings as derived from EDX spectra. The spectrum numbers correspond to the substrate numbers as in Fig. 1a. The spectra #1–6 correspond to the second series of experiments. The spectrum #7 corresponds to the coating obtained on the substrate #1 in the third series of experiments

Element	Spectrum #1		Spectrum #2		Spectrum #3		Spectrum #4	
	Weight %	At. %	Weight %	At. %	Weight %	At. %	Weight %	At. %
C	18.91	52.19	19.95	55.14	16.96	51.82	9.07	36.19
Al	1.68	2.07	1.25	1.54	0.62	0.85	-	-
Ti	60.85	42.12	55.97	38.78	52.50	40.23	50.54	50.55
Cr	0.50	0.32	0.75	0.48	1.30	0.92	2.48	2.29
Mo	-	-	-	-	2.00	0.77	3.76	1.88
Hf	4.22	0.78	11.03	2.05	15.92	3.27	23.91	6.42
Ta	8.80	1.61	5.65	1.04	5.16	1.05	4.06	1.08
W	5.04	0.91	5.39	0.97	5.53	1.10	6.16	1.61
Total	100.00	100.00	100.00	100.00	100.00	100.00	100.00	100.00
Element	Spectrum #5		Spectrum #6		Spectrum #7			
	Weight %	Weight %	Weight %	At. %	Weight %	At. %		
C	8.56	35.69	8.02	34.88	11.41	42.21		
Al	-	-	-	-	0.62	0.74		
Ti	44.79	46.85	37.24	40.63	45.52	43.03		
Cr	3.84	3.70	6.66	6.69	4.69	4.09		
Mo	7.43	3.88	14.85	8.09	7.02	3.41		
Hf	28.85	8.10	31.27	9.16	19.49	4.95		
Ta	1.48	0.41	-	-	6.55	1.04		
W	5.06	1.38	1.97	0.56	4.70	1.16		
Total	100.00	100.00	100.00	100.00	100.00	100.00		

(~ 3.8 mkm). Also, it should be noted that during first 45 min the substrate temperature was increasing up to 480 - 520 °C because of thermal radiation from the heated rod.

In the third series of experiments the coatings have been deposited onto P6M5K5 steel or sodium–calcium glass substrates. As in the previous series, at first, the upper edge of the substrate #1 together with the pipe were placed at the level of the lowest Cr disc (Fig. 1). Then the substrates were heated up to ~ 320 °C, the sputterer was turned on, and the pipe together with the substrates were gradually moving during 3.5 h until reached the location shown in Fig. 1a. In contrast with the previous experiments, in this case a multilayered composite was formed on the substrate #1 which included interlayers with gradient change of chemical elements of all the rod constituents. If to consider transition from the substrate #6 to the substrate #1, the thickness of the deposit increased from 300 nm to ~ 3.9 mkm that reflected different stages of the coating growth. So, the substrate #1 had the coating in final state. It should be mentioned that the substrate #1 temperature increased up to 520 °C simultaneously with the substrate movement.

To measure Vickers microhardness by means of MIIT-3 device, the coatings 3.2 mkm thick from second

and third series were used. Normal load onto the indenter was 0.196 N, and inaccuracy was lower than 5 %.

II. Results and discussion

2.1. Elemental composition of the coatings.

Table 1 represents numerical results of elemental composition measurements for the second series of experiments derived from obtained EDX spectra. Additionally, these data are represented in graphical form in Fig. 2 in dependence from the substrate order number. Ta concentration is not reflected in Fig. 2 because of being too small. Elemental composition distribution allows stating that carbon and titanium form the basis of the coatings. As the substrate number increases, quantity of Cr, Mo and Hf components is growing according to the elemental distribution. Increased Cr concentration in the coatings on the substrate #6 is of particular importance. Thus, chromium interlayer that is contacting with the substrate allows increasing the adhesion sufficiently [19-21].

Table 1 also indicates typical elemental composition of the coatings obtained in the third series of experiments on the substrate #1. Such coatings represent final results of the developed technology on fabricating multilayered

composites with gradient variation of chemical elements in the direction of Cr→W→Mo→Ta→Hf→Ti→C→Ti/Al→C. As in previous series, Ti and C are the major components that is a prerequisite for the carbide formation.

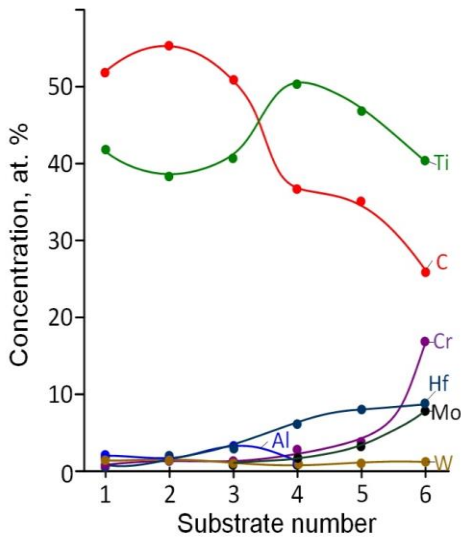


Fig. 2. Concentration of chemical elements in the coatings versus substrate number (according to Fig. 1a) for the second series of experiments.

2.2. Phase composition and microstructure of the coatings.

Fig. 3 represents X-Ray diffraction patterns for the coatings obtained in the second series of the experiments. Numbers of the patterns correspond to the numbers of the substrates. As expected from the elemental composition, TiC-based coatings are formed on the substrates #1, #2, #3 with fcc lattice of Fm3m space group, and with lattice parameters 0.4350 nm, 0.4344 nm and 0.4333 nm. These calculated values differ from the reference data (0.4327 nm for TiC) that can be explained by substitution of Ti in the lattice sites by such heavier atoms as Cr, W, Mo, Ta and Hf. Considering transition to the coatings on the substrates #4, #5, #6, intensity of the diffraction maxima decreases and their width increases considerably that depicts the process of structural disordering.

As number of the substrates changes from #4 to #6, gradual blurring of the diffraction maxima results from gradient increase of Cr, Mo, and Hf concentrations (see Fig. 2) that is accompanied by transition to the metal mixture carbide.

Phase composition of the coatings fabricated in the third series of experiments on the glass substrate #1 is also based on fcc lattice with lattice parameter close to TiC (0.4341 nm) (see Fig. 4). It should be mentioned that deposition onto the glass substrates #1, #2, #3 in the second series of experiments and onto the substrate #1 in the third series is accompanied by the growth texture which is determined by TiC (111) plane being parallel to the substrate surface. Such growth texture results from the fact that TiC (111) plane in fcc lattice has the highest packaging density and, hence, adatoms on this plane have the highest binding energy under conditions of plasma action upon the growth surface and relatively high temperature [22].

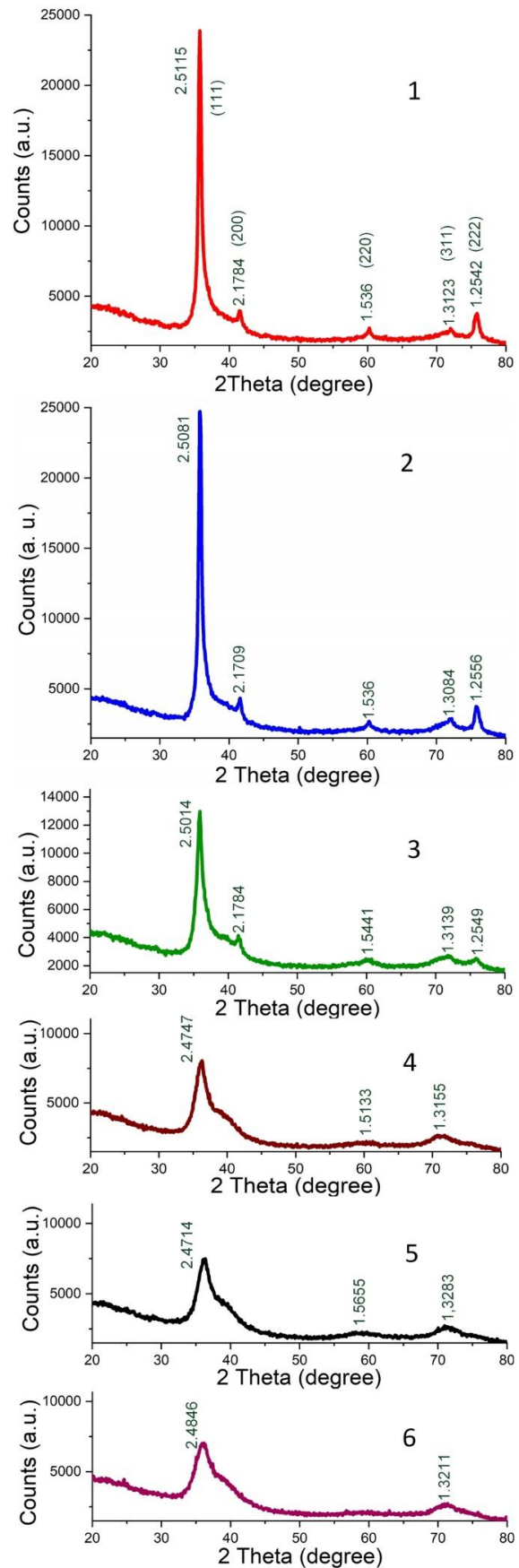


Fig. 3. XRD patterns of the coatings deposited onto glass substrates. The numbers of the patterns correspond to the numbers of the substrates in Fig. 1a

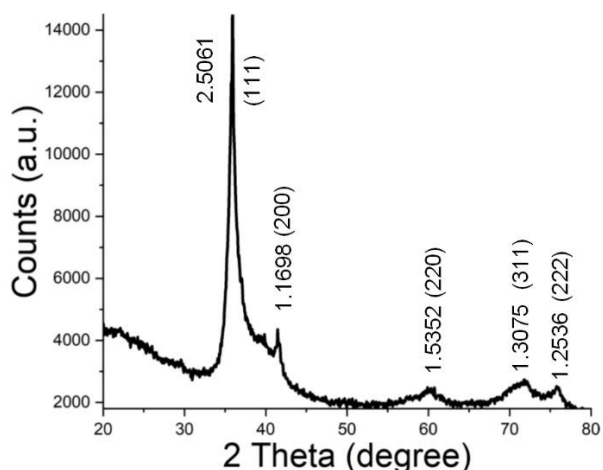


Fig. 4. XRD pattern of the coating deposited on the substrate #1 in the third series of experiments.

Results of TEM studies for the first series of experiments are shown in Fig. 5. It can be noticed that electron diffraction results are in very good agreement with XRD data. So, the thin films on the substrates #1, #2, #3 form fcc phase with the lattice period of ~ 0.43 nm. Along with it, the growth texture on initial growth stages when TiC (002) plane is parallel to KCl (002) (Fig. 5) results from the orienting action of the substrate. This differs from the growth texture of initial and further growth stages on glass substrates in other series of experiments. When forming condensates on the substrates #4, #5, #6 (Fig. 5), one can see lowering of the diffraction maxima intensity and their blurring that also correlates well with XRD studies (Fig. 3). Such process of structural disordering according to the microstructure images on Fig. 5 is also confirmed by decrease in mean sizes of crystalline grains approximately from 10 nm (on the substrate #1) to several nm (on the substrate #6).

Surface morphology of the deposited coatings is shown in Fig. 6 as SEM-images obtained in the secondary electron mode. Under maximal concentration of C and Ti in the coatings more developed surface relief is observed that is the result of bigger crystal growth. At the same time, if considering transition from the substrate #1 to the substrate #3 under almost the same amount of Ti and C (Fig. 6), the surface relief becomes less pronounced. Hence, one can conclude that structure formation is influenced not only by C and Ti concentration. In this case one should take into account higher temperature of the upper part of the rod target (see Fig. 1b) that is a prerequisite of more intense heating of the substrate #1 to the temperature of ~ 520 °C. Also, when considering transition from the substrate #4 to the substrate #6, smooth and mirror-like growth surface appears. This is caused by Cr, Hf, and Mo concentration increase (see Fig. 2) and, to some extent, by decrease in the substrate temperature to 480 °C.

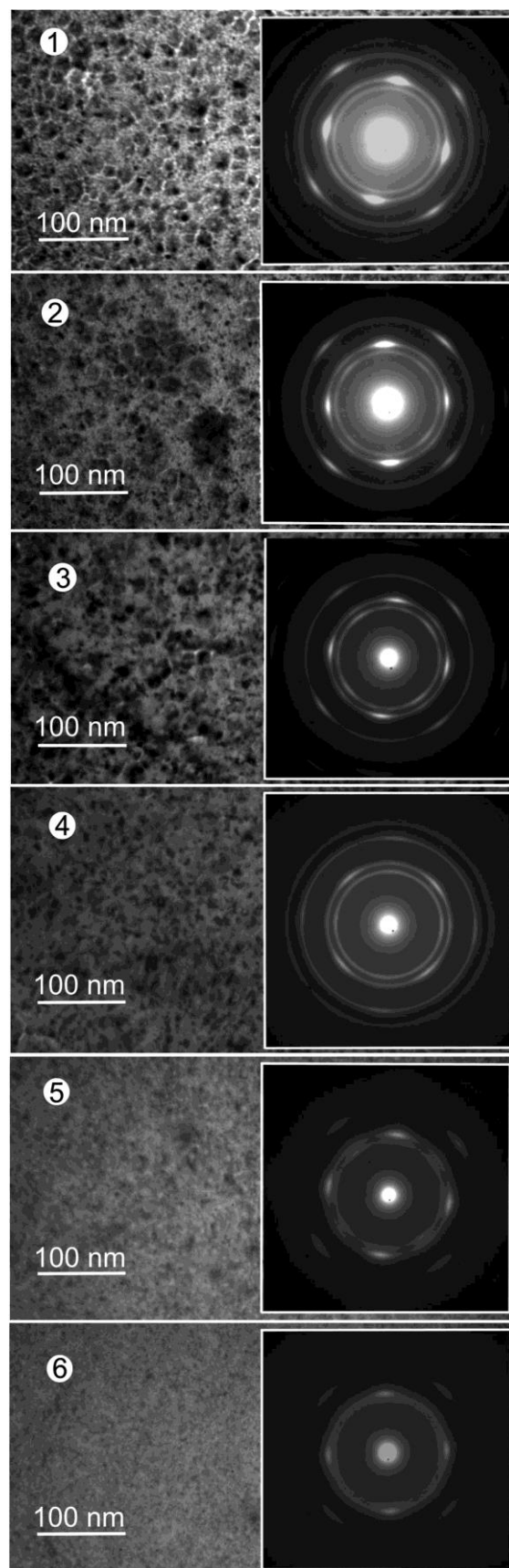


Fig. 5. TEM-images of deposited thin films and their electron diffraction patterns. The numbers of the microstructures correspond to the substrate numbers in Fig. 1a.

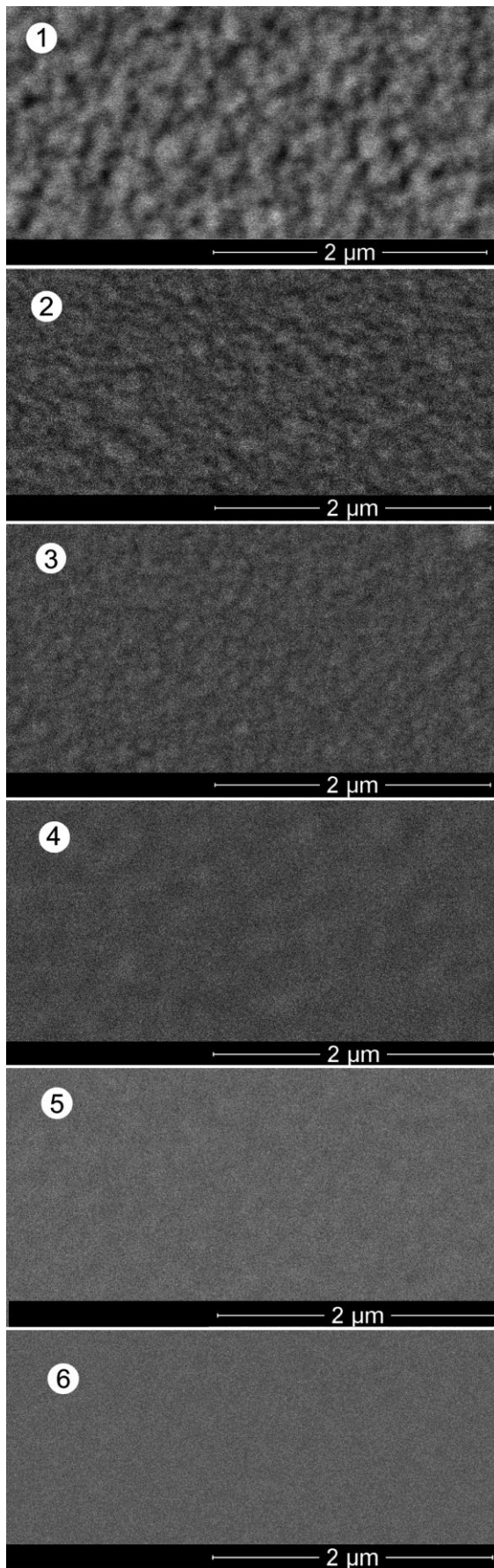


Fig. 6. SEM-images of the coatings surface morphology. The numbers of the images correspond to the substrate numbers in Fig. 1a.

2.3. Mechanical properties of the coatings.

Let us note that during the second series of experiments deposition onto the glass substrate #1 resulted sometimes in tearing of the coating fragments from the substrate together with glass pieces. It testifies to high adhesion of the Cr-enriched interlayer, on the one side, and to considerable mechanical stress at the coating-substrate interface, on the other. Mechanical stress appears since the thermal expansion coefficient α_T of sodium-calcium glass, Cr, and TiC constitute $9.2 \cdot 10^{-6}$, $9.2 \cdot 10^{-6}$ and $7.4 \cdot 10^{-6} \text{ K}^{-1}$ correspondingly [23, 24] within the temperature interval 25 - 300 °C. In this case the TiC layer reduces its dimensions much less than glass during cooling after high temperature deposition that is a prerequisite for considerable compressive stress. Since α_T of glass and Cr are the same, the stresses directly at the contact interface of the glass surface and the Cr-enriched interlayer are less pronounced that is they exist solely because of TiC layer influence. It should be mentioned that exfoliation of the coatings on the glass substrates #2-6 was rarely observed that can be explained by decreased deposition temperature and delocalization of stresses due to lowering of microhardness and transition to metal mixture carbide. At the same time, in the third series of experiments exfoliation of the coatings from P6M5K5 steel substrate was not observed. Partly, it is explained by the fact that α_T of steel is $10.5 \cdot 10^{-6} \text{ K}^{-1}$ [25] that does not lead to compressive stress and is closer to α_T of TiC.

Fig. 7 represents coatings microhardness H_μ dependence on the glass substrate number for the second series of experiments. From the shown dependence it follows that elemental composition is important for the microhardness value. Thus, the microhardness increases at transition to metal mixture carbide that is for the substrate #6. On the other side, higher increase in microhardness is observed in the coatings on the substrates #1 and #2 that can be explained by transition to TiC and increase in the deposition temperature because of heating of the growth surface by thermal radiation coming from the more heated rod. The highest measured value of microhardness constituted ~ 24 - 26 GPa and was obtained for the P6M5K5 steel substrate #1 in the third series of experiments.

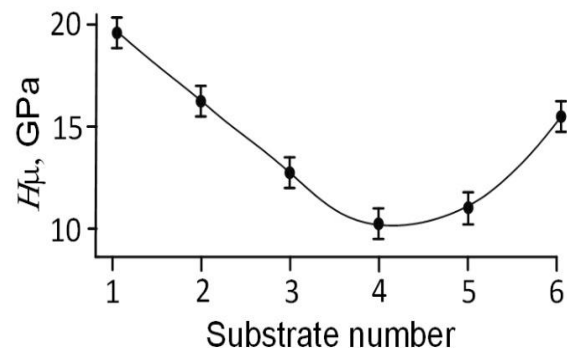


Fig. 7. Microhardness versus the substrate number (as in Fig. 1a) for the second series of experiments.

Conclusions

The presents work offers a new technology for fabricating multilayered coatings on inner surfaces of pipes. The coatings possess gradient variation of elemental composition in direction from the substrate surface to the coating surface as Cr→W→Mo→Ta→Hf→Ti→C→Ti/Al→C. The following can be concluded:

1. The indicated above gradient variation of elemental composition of the coatings creates prerequisites for high adhesion at the interface between the substrate and the Cr-enriched interlayers.

2. Based on TEM, SEM, XRD and EDX studies it is found that the above elemental distribution creates conditions for transition from metal mixture carbide with grain sizes of several nm to titanium carbide with grain sizes of ~ 8 - 15 nm. The roughness of the coatings surface increases simultaneously with the mentioned structural changes.

3. Increase in the microhardness of the coatings fabricated in the second series of experiments is determined by formation of carbide of such metals

mixture as Ti, Cr, Hf and Mo (up to ~ 16 GPa) or by increase in the TiC growth surface temperature by thermal radiation from the heated rod target (up to ~ 19 GPa). The highest microhardness (~ 26 GPa) is measured for the third series coatings fabricated on P6M5K5 steel substrates and based on the multicomponent and simultaneously multilayered composite with the mentioned above gradient variation of the elemental composition.

The work is implemented within the project "Regularities of structure formation of high-entropy multielement systems coatings on the inner surfaces of low diameter pipes" № 0118U003573 funded by State budget of Ukraine.

Perekrestov V.I. - Professor, Doctor of Technical Sciences, Chief Researcher;

Kosminska Yu.O. - Ph.D., Associate Professor;

Hannych Yu.V. - student;

Kornyushchenko G.S. - Ph.D., Associate Professor.

- [1] M.K. Samani, X.Z. Ding, N. Khosravian, B. Amin-Ahmadi, Yang Yi, G. Chen, E.C. Neyts, A. Bogaerts, B.K. Tay, *Thin Solid Films* 578, 133 (2015).
- [2] D.A. Kolesnikov, U.S. Nemchenko, V.M. Beresnev, O.V. Sobol', V.A. Novikov, S.V. Litovchenko, V.A. Stolbovoy, I.Yu. Goncharov, P.V. Turbin, L.V. Malikov, *Journal of nano- and electronic physics* 8(3), 03045-1 (2016).
- [3] V.M. Beresnev, O.V. Sobol', S.V. Litovchenko, U.S. Nemchenko, V.A. Stolbovoy, D.A. Kolesnikov, A.A. Meylekhov, A.A. Postel'nik, P.V. Turbin, L.V. Malikov, *Journal of nano- and electronic physics* 8(2), 02057-1 (2016).
- [4] U.S. Nemchenko, V.M. Beresnev, O.V. Sobol', S.V. Litovchenko, V.A. Stolbovoy, *Problems of Atomic Science and Tecnology* 1(101), 112 (2016).
- [5] V.M. Beresnev, M.Yu. Kopeykina, S.A. Klimenko, *Problems of Atomic Science and Tecnology* 1(17), 152 (2008).
- [6] D. Shinde, S. Fritze, M. Thuvander, P. Malinovskis, L. Riekehr, U. Jansson, K. Stiller, *Microscopy and Microanalysis*, 25(2), 1 (2019).
- [7] P. Malinovskis, S. Fritze, L. Riekehr, J. Cedervall, D. Rehnlund, L. Nyholm, E. Lewin, U. Jansson, *Materials & Design* 149, 51 (2018).
- [8] S. Fritze, P. Malinovskis, L. Riekehr, L. von Fieandt, E. Lewin, U. Jansson, *Scientific Reports* 8, 14508 (2018).
- [9] V. Braic, A. Vladescu, M. Balaceanu, C.R. Luculescu, M. Braic, *Surface and Coatings Technology* 211, 117 (2012).
- [10] V. Braic, M. Balaceanu, M. Braic, A. Vladescu, S. Panseri, A. Russo, *Journal of the Mechanical Behavior of Biomedical Materials* 10, 197 (2012).
- [11] V.F. Gorban, A.A. Andreyev, G.N. Kartmazov, A.M. Chikryzhov, M.V. Karpets, A.V. Dolomanov, A.A. Ostroverkh, E.V. Kantsyr, *Journal of Superhard Materials* 39, 166 (2017).
- [12] V.V. Uglov, G. Abadias, A.Y. Rovbut, S.V. Zlotski, I.A. Saladukhin, V.A. Skuratov, S. Petrovich, *Nuclear Instruments and Methods in Physics Research Section B: Beam Interactions with Materials and Atoms* 354, 269 (2015).
- [13] F.F. Komarov, A.D. Pogrebnyak, S.V. Konstantinov, *Technical Physics* 60(10), 1519 (2015).
- [14] A.D. Pogrebnyak, I.V. Yakushchenko, O.V. Bondar, O.V. Sobol', V.M. Beresnev, K. Oyoshi, Y. Takeda, *Technical Physics Letters* 41(11), 1054 (2015).
- [15] E.N. Kabulov, *Aviation Materials and Technologies* 1(34), 3 (2015).
- [16] Yu.O. Kosminska, V.I. Perekrestov, G.S. Korniyushchenko, *Metallophysics and Advanced Technologies* 41(6), 733 (2019).
- [17] V.I. Perekrestov, S.N. Kravchenko, Yu.A. Kosminskaya, I.N. Kononenko, *Metallophysics and Advanced Technologies* 33(2), 203 (2011).
- [18] V.I. Perekrestov, S.N. Kravchenko, *Instruments and Experimental Techniques* 3, 123 (2002).
- [19] W.Q. Qiu, Z.W. Liu, L.X. He, D.C. Zeng, Y.-W. Mai, *Materials Letters* 81, 155 (2012).

- [20] K.-D. Bouzakis, S. Makrimalakis, G. Katirtzoglou, G. Skordaris, S. Gerardis, E. Bouzakis, W. Koelker, *Surface and Coatings Technology*, 205(5), 1564 (2010).
- [21] D. Li, S. Guruvenket, S. Hassani, V. Bousser, M. Azzi, J. A. Szpunar, J. E. Klemberg-Sapieha, *Thin Solid Films* 519(10), 3128 (2011).
- [22] V.I. Perekrestov, A.S. Korniyushchenko, Yu.A. Kosminskaya, *Technical Physics* 53(10), 1364 (2008).
- [23] V.G. Samsonov, I.M. Vinitskiy, *Tugoplavkiye soyedineniya (Metallurgiya, Moscow, 1976)*.
- [24] A.S. Yenokhovich, *Spravochnik po fizike (Prosveshcheniye, Moscow, 1990)*.
- [25] L.A. Pozdnyak, *Instrumental'nyye stali: Spravochnik (Metallurgiya, Moscow, 1977)*.

В.І. Перекрестов, Ю.О. Космінська, Ю.В. Ганніч, Г.С. Корнющенко

Закономірності структуроутворення та фізичні властивості багат шарових композитів на основі W, Ta, Hf, Ti, Mo, Cr, Al та C

Сумський державний університет, м. Суми, Україна, v.perekrestov@phe.sumdu.edu.ua

Запропонована нова технологія отримання багат шарових композитів на внутрішній поверхні труби шляхом іонного розпилення стрижня, складеного з різних металів та графіту. Установлено, що за умови градієнтної зміни елементного складу композиту у напрямку Cr→W→Mo→Ta→Hf→Ti→C→Ti/Al→C відбувається перехід від карбїду суміші металів з середніми розмірами зерен декілька одиниць нанометрів до TiC із розмірами зерен ~ 8 - 15 нм. З'ясовано, що підвищення мікротвердості до ~ 26 ГПа визначається додатковим розігрівом поверхні нарощування тепловим випромінюванням розігрітого іонами стрижня та елементним складом прошарків композиту.

Ключові слова: багаткомпонентні покриття, композит, вуглець, карбїд, елементний склад, фазовий склад.